

# CamoSAM2: Motion-Appearance Induced Auto-Refining Prompts for Video Camouflaged Object Detection

Xin Zhang  
National Key Laboratory of  
Fundamental Science on Synthetic Vision,  
Sichuan University  
zhangxinchina1314@gmail.com

Keren Fu, Qijun Zhao  
College of Computer Science,  
National Key Laboratory of  
Fundamental Science on Synthetic Vision,  
Sichuan University  
fkrsuper@scu.edu.cn, qjzhao@scu.edu.cn

## Abstract

The Segment Anything Model 2 (SAM2), a prompt-guided video foundation model, has remarkably performed in video object segmentation, drawing significant attention in the community. Due to the high similarity between camouflaged objects and their surroundings, which makes them difficult to distinguish even by the human eye, the application of SAM2 for automated segmentation in real-world scenarios faces challenges in camouflage perception and reliable prompts generation. To address these issues, we propose CamoSAM2, a motion-appearance prompt inducer (MAPI) and refinement framework to automatically generate and refine prompts for SAM2, enabling high-quality automatic detection and segmentation in VCOD task. Initially, we introduce a prompt inducer that simultaneously integrates motion and appearance cues to detect camouflaged objects, delivering more accurate initial predictions than existing methods. Subsequently, we propose a video-based adaptive multi-prompts refinement (AMPR) strategy tailored for SAM2, aimed at mitigating prompt error in initial coarse masks and further producing good prompts. Specifically, we introduce a novel three-step process to generate reliable prompts by camouflaged object determination, pivotal prompting frame selection, and multi-prompts formation. Extensive experiments conducted on two benchmark datasets demonstrate that our proposed model, CamoSAM2, significantly outperforms existing state-of-the-art methods, achieving increases of 8.0% and 10.1% in mIoU metric. Additionally, our method achieves the fastest inference speed compared to current VCOD models.

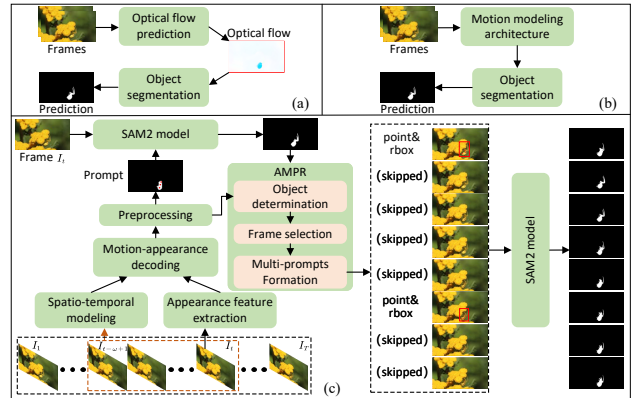


Figure 1. Illustration of previous VCOD methods (a-b) with ours (c): (a) Feeding optical flow maps directly [24, 45]; (b) Learning implicit motion cues from adjacent frames [5]; (c) Learning motion-appearance guided prompts and subsequently refines these prompts automatically to enhance the effectiveness of SAM2.

## 1. Introduction

Camouflaged object detection (COD) seeks to identify and segment *hidden objects* that blend seamlessly into their surroundings. This task is critical in computer vision with a wide range of applications, including surveillance [27], medical image analysis [10, 20, 42, 43], and wildlife conservation [26]. While significant progress has been made in detecting camouflaged objects from a single image, some camouflages in nature remain nearly imperceptible in static scenes, even to the most perceptive predators. However, once the concealed prey moves, the concealment is disrupted, making them susceptible to a predator’s attack. This natural phenomenon has inspired research into harnessing motion cues to tackle the challenges of camouflaged object detection in videos.

As illustrated in Figure 1, existing VCOD methods predominantly focus on modeling the motion relationships be-

tween adjacent frames, either explicitly (a) or implicitly (b), to facilitate camouflaged object detection. While these methods have shown encouraging results, the limited availability of training data often results in overfitting and poor generalization to unseen scenarios. Recently, the visual foundation model segment anything model (SAM) [23] has demonstrated remarkable generalization capabilities in natural image segmentation tasks. Building on this, Hui *et al.* [18] leveraged temporal and spatial relationships between frames to generate masks and bounding boxes that serve as prompts for SAM. While this approach eliminates the need for manual prompt inputs in SAM, it does not address the issue of temporal consistency in predictions, essentially degrading to a single-frame prediction method utilizing SAM. In contrast, Meeran *et al.* [30] utilized the SAM image encoder as a feature extraction backbone and introduced a propagation module to extend the initial user-provided mask across subsequent frames, thereby addressing the temporal consistency of predictions. However, this approach requires user-provided high-quality object masks in the first frame, which is both challenging and time-intensive to obtain in practical scenarios.

Recently, SAM2 [36] has emerged as a significant advancement in video object segmentation, demonstrating consistent performance across various tasks [25, 39, 51]. Leveraging SAM2’s impressive versatility, this work aims to adapt it for VCOD in a fully automated manner (*i.e.*, no any user labeling or interaction is needed). In those camouflaged scenarios, SAM2’s effectiveness in identifying specific regions depends heavily on the quality and precision of the provided prompts. However, generating good prompts is challenging, especially without needing user input.

In video-based tasks, both temporal-spatial relationships and appearance cues play equally critical roles in effective target detection. This underscores the importance of motion-appearance induced prompts specifically designed for SAM2 to enhance its effectiveness in video camouflaged object detection. Moreover, challenges such as occlusions, camera shake, and scene transitions, can undermine the reliability of learned prompts, potentially degrading performance. Motivated by these considerations, we propose a novel method that autonomously generates and refines prompts, empowering SAM2 to produce reliable and robust segmentation results. To the best of our knowledge, the proposed CamoSAM2 is the first SAM2-based approach specifically tailored for video camouflaged object detection.

The main contributions are summarized as follows:

- We introduce MAPI, which simultaneously leverages motion and appearance cues to generate a series of prompts for subsequent SAM2, facilitating the identification of camouflaged objects in videos without the need for user-provided prompts.
- To mitigate initial coarse mask errors introduced by

MAPI, we propose a video-based adaptive multi-prompts refinement approach, AMPR, which operates without additional training parameters. AMPR automatically identifies pivotal frames for prompt generation, refining bounding boxes with point-based prompts to produce reliable and robust multi-prompts configurations.

- Extensive experiments on the MoCA-Mask and CAD datasets demonstrate that the proposed CamoSAM2 achieves significant performance gains over state-of-the-art model SAM-PM [30], with mIoU improvements of 8.0% and 10.1%, respectively.

## 2. Related Work

### 2.1. Image-based COD

Methods in this category focus on detecting camouflaged objects within a single RGB image. Inspired by natural predatory behaviors, approaches such as SINet-V2 [11] and PFNet [31] employ a coarse-to-fine strategy. These methods initially generate a preliminary map to locate potential camouflaged objects, which is then progressively refined for accurate segmentation. To further improve detection performance, Zhai *et al.* [47] introduced an auxiliary task that integrates classification or boundary detection with camouflaged object detection. Additionally, Jia *et al.* [21] proposed the SegMaR framework, an iterative refinement approach designed to locate, magnify, and detect camouflaged objects. Khan *et al.* [22] introduced a feature split and context refinement network to refine camouflaged features. Yao *et al.* [46] designed a graph interaction network to discover camouflaged objects effectively. Several studies [6, 13, 38, 50] leveraged frequency-learning modules to extract subtle foreground-background cues by decomposing features into multiple frequency components, thus enhancing spatial identification.

### 2.2. Video-based COD

For VCOD task, motion cues are essential for effective detection. Bidau *et al.* [1] introduced a method by approximating various motion models derived from dense optical flow. Lamdouar *et al.* [24] introduced a video registration and segmentation network for detecting camouflaged objects, leveraging optical flow and difference images as inputs. However, the reliance on imprecise optical flow can lead to cumulative errors in mask prediction. To address this issue, Cheng *et al.* [5] developed a two-stage model that implicitly captures and utilizes motion information. Subsequently, to eliminate inaccuracies stemming from implicit motion modeling in SLT-Net [5], Hui *et al.* [17] introduced a motion-induced consistency preserving approach between frames with a feature pyramid framework. More recently, efforts have been directed toward adapting SAM for VCOD tasks. Hui *et al.* [18] leveraged temporal and spatial re-

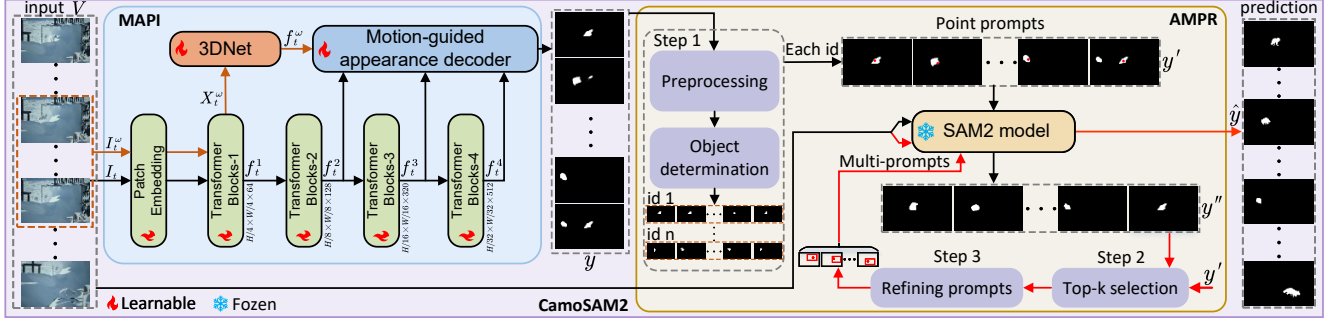


Figure 2. Pipeline of our CamoSAM2, which consists of two main components: motion-appearance prompt inducer (MAPI) and video-based adaptive multi-prompts refinement (AMPR). The fire and snowflake symbol signifies that the model parameters in this part are kept learnable and frozen, respectively.

relationships between frames to generate mask and bounding box prompts for interaction with SAM. Additionally, Meeran *et al.* [30] utilized the SAM image encoder as a feature extraction backbone and introduced a module to propagate the initial ground truth mask across subsequent frames. Compared to existing approaches, our method integrates both motion and appearance cues to autonomously generate and refine reliable prompts for SAM2, enabling optimized performance without the need for user-provided prompts.

### 2.3. Segment Anything Model

The Segment Anything Model (SAM) [23] has demonstrated remarkable performance in natural image segmentation, particularly due to its robust zero-shot capabilities. However, SAM’s effectiveness can vary significantly across specialized domains [3]. For instance, it faces challenges in segmenting medical images [15] and detecting camouflaged objects [40]. To expand SAM’s applicability in medical imaging, approaches like MedSAM [28] and SAM-Adapter [2] have been developed, integrating domain-specific knowledge to improve performance. Building on SAM’s success in the image domain, Meta AI Research introduced SAM2 [36], a unified architecture designed for both image and video segmentation tasks. This advancement has prompted further research, with methods such as MedSAM2 [51] and SAM2-Adapter [4] integrating specialized knowledge to tailor SAM2 for specific applications. However, to date, no efforts have been made to adapt SAM2 for the VCOD task. To bridge this gap, we introduce a novel framework that employs motion- and appearance-guided prompts, alongside an automatic multi-prompts optimization mechanism specifically designed for SAM2. Our proposed framework marks a pioneering application of SAM2 in video camouflaged object detection.

## 3. Proposed Method

The overall architecture of our proposed CamoSAM2 is illustrated in Figure 2. The framework is composed of two

main components: (1) **Motion-Appearance Prompt Inducer (MAPI)**, which includes modules for appearance feature extraction, motion perception, and a motion-guided appearance decoder; and (2) **Video-based Adaptive Multi-Prompts Refinement (AMPR)**, which operates through three progressive stages: camouflaged targets determination, pivotal prompting frame selection, and multi-prompts formation. Each of these components will be detailed in the following sections.

### 3.1. Motion-Appearance Prompt Inducer

It is well-known that SAM2 relies on user-provided prompts to segment specific regions. However, accurately identifying camouflaged objects is challenging, making it difficult to supply reliable visual prompts. Additionally, reliance on user input limits the applicability of SAM2 in real-world scenarios. To address these issues, we propose a motion-appearance prompt inducer MAPI that enables SAM2 to automatically detect camouflaged objects without external user-provided prompts.

#### 3.1.1. Appearance Feature Extraction

Appearance information encompasses the visual characteristics of an object, including color, texture, and shape. This information is crucial for discerning the subtle differences between camouflaged objects and their backgrounds. Vision transformer-based models [5, 11, 16–18, 32] have demonstrated impressive capabilities in modeling both global and local contexts for the task of detecting camouflaged objects in images. Notably, the design of the appearance feature extraction network is not the primary focus of this paper; therefore, for fair comparisons, we employ the PVT [41] as our feature extraction backbone, adhering to the same configurations as those in [5, 18] without additional modifications. Specifically, for a given reference frame  $I_t$ , we extract a set of features  $\{f_t^i \in \mathbb{R}^{H/2^{i+1} \times W/2^{i+1} \times C_i}, i = 1, \dots, 4\}$  at varying scales from PVT. Here,  $W$ ,  $H$ , and  $C$  denote the width, height, and channel number, respectively.

### 3.1.2. Motion Perception

Camouflaged objects closely resemble their surroundings, making them difficult to detect, even for the human eye. However, any movement from the target can disrupt this concealment, revealing its presence. Leveraging this, we incorporate motion information to enhance localization.

As shown in Figure 2, for a video sequence  $I_t^\omega \in \mathbb{R}^{\omega \times H \times W \times 3}$  of length  $\omega$  corresponding to the current frame  $I_t$ , we first feed it into the initial block of PVT backbone to obtain the low-level feature map  $X_t^\omega \in \mathbb{R}^{\omega \times H/4 \times W/4 \times 64}$ . Then we apply a 3D convolutional neural network (3DNet) to capture the temporal-spatial relationships across frames:

$$f_t^\omega = \text{3DNet}(X_t^\omega) \quad (1)$$

where  $f_t^\omega \in \mathbb{R}^{1 \times H/32 \times W/32 \times 512}$  represents the temporal-spatial relationships within  $\omega$  consecutive frames. Referring to the long-term setting of SLT-Net [5], we set  $\omega$  to 5 in this paper. The 3DNet consists of four sequential 3D convolutional blocks, each followed by activation functions and incorporating residual connections. Specifically, each block operates as follows:

$$f = x + \phi(\text{BN}(\text{Conv3D}(x))), \quad (2)$$

where  $x$  and  $f$  denote the input and output, respectively. Conv3D is  $3 \times 3 \times 3$  convolution.  $\phi$  represents the ReLU activation function [14] and BN indicates batch normalization.

### 3.1.3. Motion-guided Appearance Decoder

To effectively integrate motion and appearance information for obtaining robust masks, we employ a multi-stage fusion and decoding strategy, as illustrated in Figure 3. Initially, we apply separate  $3 \times 3$  convolutional layers to reduce the channel dimensions of features  $f_t^\omega, f_t^2, f_t^3, f_t^4$  to 64 channels. Next, the motion feature  $f_t^\omega$  is resized to match the spatial resolution of the corresponding appearance feature map  $f_t^2, f_t^3, f_t^4$ . These features are then fused through element-wise multiplication and concatenation, followed by a  $3 \times 3$  convolutional layer. To address the challenges of detecting small objects, which often lose clarity in down-sampled feature maps, and recognizing that motion features are primarily beneficial for localization, we establish feature interactions that progress from coarse to fine resolutions. The final feature map is derived using a Sigmoid activation function, with additional supervision applied to enhance robustness. Thus, for a video sequence of length  $T$ , the initial output masks of our MAPI can be mathematically expressed as:  $\mathbf{y} = \{y_1, y_2, \dots, y_T\}$ .

## 3.2. Video-based Adaptive Multi-Prompts Refinement

The motion-appearance prompt inducer MAPI leverages both single-frame appearance cues and long-range inter-frame motion to strengthen spatial identification. However,

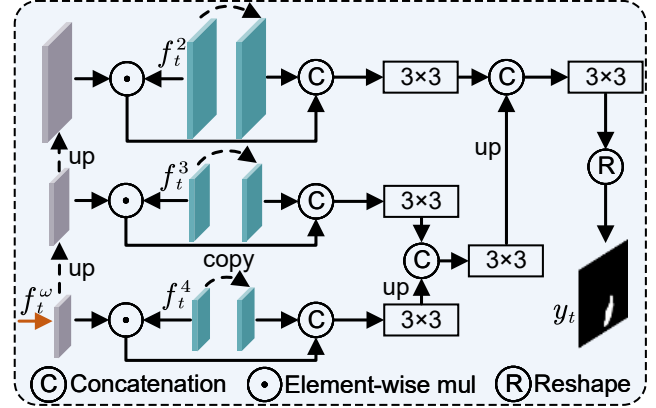


Figure 3. Structure of motion-guided appearance decoder.

this reliance on appearance and motion makes the model susceptible to temporal-spatial discontinuities, such as occlusions, camera shakes, and scene changes, which can undermine the robustness of the learned masks.

Notably, SAM2 enables prompt provision for any frame within a video sequence, offering flexibility for handling camouflaged objects. Certain frames within the sequence may exhibit stronger appearance features or more distinctive motion cues, making them essential for accurate identification and segmentation. Therefore, it is critical to identify these key frames to enable SAM2 to enrich target features and maintain long-range consistency, thereby reducing the risk of target loss. Additionally, refining prompts on these key frames is essential to further enhance their reliability. To address these challenges, we propose a parameter-free, video-based adaptive multi-prompts refinement method comprising three main steps:

**Step 1: Camouflaged object determination.** To address boundary ambiguity caused by camouflaged objects blending with backgrounds, we refine MAPI’s initial masks  $\mathbf{y}$  through a two-step process: 1) Binarization removes low-confidence edge pixels (pixel value  $\leq \tau$ ) to suppress noise and emphasize high-confidence regions near the object center ( $\tau$  is set to 127). 2) Morphological closing eliminates residual background artifacts and pseudo-targets, yielding refined masks  $\mathbf{y}'$ . We then estimate target count by analyzing the connected-region frequency across frames. Notably, for scenarios that are estimated to be single target, a top- $k$  frame selection filters out multi-region noisy frames (which inherently exhibit low similarity in Step 2), preventing their selection as prompt frames. Multi-target cases trigger our ID assignment protocol (Algorithm 1). Due to the space limit, more explanation and visualization of this operation can be seen in the supplementary materials (Supp).

**Step 2: Pivotal prompting frame selection.** For SAM2, point prompts offer a practical and user-friendly approach, eliminating the need for specialized knowledge and

facilitating real-world applicability. As shown in Figure 2, we generate random prompt points based on  $\mathbf{y}'$  and feed these points, along with their respective RGB images, into SAM2 to obtain single-frame predictions  $\mathbf{y}''$ . Each prediction in  $\mathbf{y}''$  is then compared against the corresponding one in  $\mathbf{y}'$  to assess similarity. To enhance computational efficiency, we employ Intersection over Union (IoU) as the similarity metric. This comparison is performed across all frames in the video clip, allowing us to rank frames by similarity and select the top- $k$  frames with the highest scores.

**Step 3: Multi-prompts formation.** For the selected top- $k$  frames, we refine prompt boxes to address under-segmentation caused by point prompts’ tendency to focus on local regions. Initially, prompt boxes are generated from SAM2’s segmentation masks  $\mathbf{y}''$  using randomly chosen points, with the boxes initialized as the minimum enclosing rectangles around these masks. Given that the initial prediction results  $\mathbf{y}''$  are typically smaller than the ground truth (GT) due to the point prompt potentially guiding the model to segment only local regions rather than the entire target object, each box is expanded outward in four directions—up, down, left, and right. The expansion process proceeds in each direction until a significant change is observed, which then serves as the stopping criterion for that direction. This process is repeated for all four directions until the final bounding box is established. Finally, the optimized boxes, along with their respective prompt points and frames, are then inputted back into SAM2 to produce final predictions:  $\hat{\mathbf{y}} = \{\hat{y}_1, \hat{y}_2, \dots, \hat{y}_T\}$ . The visual optimization process for the pivotal frame  $i$ , transitioning from  $y_i''$  to  $\hat{y}_i$  is illustrated in Figure 5. This progression involves transforming “Point” into “Point+Box”, and subsequently into “Point+Rbox”.

### 3.3. Supervision and Loss Function

We perform joint optimization of the prompt inducer with both motion and appearance cues by minimizing a hybrid loss function [12], defined as follows:

$$\mathcal{L}_{\text{pred}} = \mathcal{L}_{\text{IoU}} + \mathcal{L}_{\text{bce}} + \mathcal{L}_{\text{e-loss}}, \quad (3)$$

where  $\mathcal{L}_{\text{IoU}}$ ,  $\mathcal{L}_{\text{bce}}$ , and  $\mathcal{L}_{\text{e-loss}}$  denote IoU loss, binary cross-entropy loss, and enhanced-alignment loss, respectively.

---

#### Algorithm 1 The proposed AMPR

---

- 1: **Input:** Video  $V = \{I_1, \dots, I_T\}$ ; Initial masks  $\mathbf{y} = \{y_1, \dots, y_T\}$ ; Thresholds  $\tau, \beta$ ; Hyperparameters  $\alpha, m$
- 2: **Output:** Final predictions  $\hat{\mathbf{y}} = \{\hat{y}_1, \dots, \hat{y}_T\}$
- 3: **Step 1: Camouflaged object determination**
- 4: Initialize  $\mathcal{C} \leftarrow \emptyset$  to store region counts
- 5: **for**  $t = 1$  to  $T$  **do**
- 6:   Binarize mask  $y_t'$ , apply morphological closing
- 7:   Compute connected regions  $R_t$ , let  $n_t = |R_t|$
- 8:   Update dictionary:  $\mathcal{C}(n_t) \leftarrow \mathcal{C}(n_t) + 1$
- 9: **end for**
- 10:  $N_{\text{max}} \leftarrow \arg \max_{n_t} \mathcal{C}(n_t)$
- 11: Assign IDs to targets in  $I_x$  based on  $\mathcal{C}(n_t) = N_{\text{max}}$
- 12: **for** each subsequent frame  $I_t$  **do**
- 13:   **for** each target ID from  $I_{t-1}$  **do**
- 14:     Match targets using IoU (IoU  $> \tau$ )
- 15:   **end for**
- 16: **end for**
- 17: Repeat similar steps for previous frames
- 18: **Step 2: Pivotal prompting frame selection**
- 19: **for** each target ID **do**
- 20:   **for** each frame  $I_t$  **do**
- 21:     Input  $m$  prompt points  $P_t$  into SAM2 to obtain  $y_t''$
- 22:   **end for**
- 23: **end for**
- 24: Select top  $k$  frames:  $I_{\text{selected}} = \text{Top-}k(\text{IoU}(y_t', y_t''))$
- 25: **Step 3: Multi-prompts formation**
- 26: **for** each selected frame  $I_t$  **do**
- 27:   Generate initial box  $B_t$  around  $y_t''$
- 28:   **for** each direction (up, down, left, right) **do**
- 29:     **repeat**
- 30:       Expand box  $B_t$  with step size  $\alpha$
- 31:       Compute mask change  $\Delta M$
- 32:       **until**  $\Delta M \geq \beta$
- 33:     **end for**
- 34:   Save final box  $B_t$
- 35: **end for**
- 36: Input  $\mathbb{B} = \{B_a, \dots, B_n\}$ ,  $\mathbb{P} = \{P_a, \dots, P_n\}$ , and  $I_{\text{selected}} = \{I_a, \dots, I_n\}$  into SAM2 to get final predictions:  $\hat{\mathbf{y}} = \text{SAM2}(\mathbb{B}, \mathbb{P}, I_{\text{selected}})$

---

## 4. Experiment Results and Analyses

### 4.1. Datasets and Metrics

**Datasets.** Following previous VCOD methods [5, 17, 18, 30], we conduct experiments on two widely recognized VCOD benchmarks: MoCA-Mask [5] and CAD [1]. MoCA-Mask is recognized as the more challenging dataset, featuring camouflaged animals in natural environments. It consists of 19,313 frames derived from 71 video clips for training and 3,626 frames from 16 clips for testing. Conversely, the CAD dataset is a smaller collection specifically

for testing, comprising 836 frames from 9 clips sourced from YouTube videos.

**Evaluation metrics.** We adopt widely recognized evaluation metrics to assess our model performance, namely: structure measure ( $S_\alpha$ ) [7], weighted F-measure ( $F_\beta^w$ ) [29], enhanced-alignment measure ( $E_\phi$  [8]), mean absolute error ( $\mathcal{M}$ ) [34], and mean value of Dice (mDice) and IoU (mIoU). These metrics provide a comprehensive and reliable assessment of model performance.

**Implementation details.** Our CamoSAM2 is implemented by PyTorch [33] on a single NVIDIA 4090 GPU and optimized with Adam optimizer by cosine annealing strategy, whose maximum, minimum learning rates, and the maximum adjusted iteration are set to  $1e-5$ ,  $1e-6$ , and 20, respectively. The parameters  $\tau, \alpha, \beta, m$  in Algorithm 1 are set to 0.5, 5,  $5e-4$ , and 5, respectively. For fair comparisons, we strictly follow the training configurations detailed in [5, 18], employing PVT [41] as the feature extraction backbone. And the PVT backbone is also pre-trained on the static training set of COD10K (3,040 images) [11]. All input images are resized to  $352 \times 352$ . The model is trained on the training set of MoCA-Mask (19,313 frames) [5] and evaluated on the MoCA-Mask test set, as well as on the entire CAD dataset. The mini-batch is set to 6, and MAPI trains for 4 hours over 60 epochs. We choose the hierarchical version of SAM2 in all our experiments. To ensure robust results, all experiments were conducted five times, with the median result reported in the following tables.

## 4.2. Quantitative and Qualitative Comparison

To evaluate the effectiveness of the proposed CamoSAM2, we compare it against a range of state-of-the-art methods, including both image-based and video-based approaches. As shown in Table 1, the results reveal several key insights: (i) The substantial performance gap between video-based and single-image camouflaged object detection methods highlights the critical role of temporal-spatial relationships in resolving video camouflaged challenges. (ii) SAM-based methods achieve superior performance relative to other approaches, underscoring the powerful feature extraction and generalization capabilities of the foundation model. (iii) Our motion-appearance prompt inducer outperforms all existing non-SAM-based models in predicting camouflaged objects, showcasing the effectiveness of our simple yet powerful design in extracting and integrating both motion and appearance features. (iv) The proposed CamoSAM2 outperforms all video-based camouflaged object detection methods. Notably, it achieves a 6.2% improvement in  $S_\alpha$  on the CAD dataset over the previous state-of-the-art SAM-PM [30], suggesting that our CamoSAM2 exhibits enhanced robustness and generalization on unseen dataset. Furthermore, visual comparisons in Figure 4 show that our CamoSAM2 more accurately

localizes and segments camouflaged targets compared to other leading methods. To demonstrate consistent success across consecutive frames, we offer additional per-frame qualitative results in the [Supp.](#)

Additionally, we present the model parameter count and frames-per-second (FPS). As detailed in Table 2, our model achieves a 72.2% improvement in mDice with only a 59.18M increase in parameters over SLT-Net. Notably, our model also achieves the highest FPS among existing VCOD models, underscoring its efficiency and effectiveness. To further validate the generalizability of our AMPR, we apply it to existing VCOD methods. The variants of these models show improved performance compared to their original versions (See details in [Supp.](#)). This demonstrates that the incorporation of AMPR can substantially enhance the performance of a VCOD model, even when the baseline model is not particularly strong. Furthermore, when applied to a more robust model, such as our MAPI, the AMPR generates even better results, underscoring the close interdependence between these two designed components in our method.

## 4.3. Ablation Studies

To comprehensively assess the effectiveness of the key components and the selection of hyperparameters, we perform an in-depth analysis by decoupling the core design and varying hyperparameter values.

**Ablation analysis of MAPI.** Table 3 evaluates the segmentation results of MAPI by progressively incorporating each module. The ‘‘Baseline’’ refers to using only the final layer of the PVT backbone for predictions. The ‘‘Appearance’’ configuration decodes multi-layer feature maps from different stages of the backbone to generate predictions. As observed, decoding multi-stage appearance features significantly enhances performance. When motion information is introduced (row 3, our MAPI), the mDice metric notably improves from 0.341 to 0.399, demonstrating the critical role of inter-frame motion in breaking camouflage. Additionally, in comparison to the results in Table 1, MAPI outperforms all previous non-SAM-based methods, further underscoring the effectiveness of our design.

**Prompt frame selection.** Table 4 evaluates the impact of different frame selection schemes on MoCA-Mask dataset. Three prompt selection strategies are compared: using the first frame of a video sequence (‘‘First’’), a randomly chosen frame (‘‘Random’’), and the frame selected by our proposed strategy (‘‘Top-1’’), with each prompted frame accompanied by a single random prompt point. The ‘‘Top-1’’ outperforms both the ‘‘First’’ and ‘‘Random’’ selections across all metrics with substantial improvements. This demonstrates that selecting the appropriate prompt frame (‘‘Top-1’’) enhances segmentation accuracy, as it likely captures the most informative features for describing the object. In contrast, the ‘‘First’’ performs the worst, indicating that simply us-

Model	Publication	Input	MoCA-Mask						CAD					
			$S_\alpha \uparrow$	$F_\beta^w \uparrow$	$E_\phi \uparrow$	$\mathcal{M} \downarrow$	mDice $\uparrow$	mIoU $\uparrow$	$S_\alpha \uparrow$	$F_\beta^w \uparrow$	$E_\phi \uparrow$	$\mathcal{M} \downarrow$	mDice $\uparrow$	mIoU $\uparrow$
EGNet [49]	ICCV-2019	Image	0.574	0.110	0.574	0.035	0.143	0.096	0.619	0.298	0.666	0.044	0.324	0.243
BASNet [35]	CVPR-2019	Image	0.561	0.154	0.598	0.042	0.190	0.137	0.639	0.349	0.773	0.054	0.393	0.293
PraNet [10]	MICCAI-2020	Image	0.614	0.266	0.674	0.030	0.311	0.234	0.629	0.352	0.763	0.042	0.378	0.290
SINet [9]	CVPR-2020	Image	0.574	0.185	0.655	0.030	0.221	0.156	0.601	0.204	0.589	0.089	0.289	0.209
SINet-v2 [11]	TPAMI-2021	Image	0.571	0.175	0.608	0.035	0.211	0.153	0.544	0.181	0.546	0.049	0.170	0.110
ZoomNet [32]	CVPR-2022	Image	0.582	0.201	0.682	0.026	0.236	0.197	0.661	0.235	0.666	0.089	0.345	0.265
BGNet [37]	IJCAI-2022	Image	0.590	0.203	0.647	0.023	0.225	0.168	0.651	0.240	0.625	0.077	0.320	0.238
FEDERNet [13]	CVPR-2023	Image	0.555	0.198	0.542	0.049	0.192	0.152	0.604	0.233	0.725	0.061	0.361	0.301
FSPNet [16]	CVPR-2023	Image	0.565	0.186	0.610	0.044	0.238	0.167	0.609	0.224	0.664	0.056	0.315	0.235
PUNet [48]	TIP-2023	Image	0.594	0.204	0.619	0.037	0.300	0.212	0.673	0.427	0.803	0.034	0.499	0.389
SAM2-adapter [4]	arXiv-2024	Image	0.569	0.162	0.586	0.041	0.213	0.144	0.650	0.387	0.746	0.043	0.442	0.329
FSEL [38]	ECCV-2024	Image	0.596	0.260	0.677	0.053	0.219	0.151	0.649	0.368	0.732	0.053	0.434	0.325
HGINet [46]	TIP-2024	Image	0.610	0.251	0.726	0.030	0.303	0.221	0.680	0.437	0.821	0.050	0.501	0.392
RCRNet [44]	ICCV-2019	Video	0.555	0.138	0.527	0.033	0.171	0.116	0.627	0.287	0.666	0.048	0.309	0.229
PNS-Net [19]	MICCAI-2021	Video	0.576	0.134	0.562	0.038	0.189	0.133	0.678	0.369	0.720	0.043	0.409	0.308
MG [45]	ICCV-2021	Video	0.530	0.168	0.561	0.067	0.181	0.127	0.594	0.336	0.691	0.059	0.368	0.268
SLT-Net [5]	CVPR-2022	Video	0.631	0.311	0.759	0.027	0.360	0.272	0.696	0.481	<b>0.845</b>	0.030	0.493	0.401
IMEX [17]	TMM-2024	Video	0.661	0.371	0.778	0.020	0.409	0.319	0.684	0.452	0.813	0.033	0.469	0.370
TSP-SAM [18]	CVPR-2024	Video	<b>0.689</b>	<b>0.444</b>	<b>0.808</b>	<b>0.008</b>	<b>0.458</b>	<b>0.388</b>	<b>0.704</b>	<b>0.524</b>	<b>0.912</b>	<b>0.028</b>	<b>0.543</b>	<b>0.438</b>
SAM-PM [30]	CVPR-2024	Video	<b>0.728</b>	<b>0.567</b>	<b>0.813</b>	<b>0.009</b>	<b>0.594</b>	<b>0.502</b>	<b>0.729</b>	<b>0.602</b>	0.746	<b>0.018</b>	<b>0.594</b>	<b>0.493</b>
<b>MAPI</b>	Ours	Video	0.670	0.376	0.782	0.014	0.413	0.330	0.709	0.513	0.824	0.029	0.530	0.413
<b>CamoSAM2</b>	Ours	Video	<b>0.765</b>	<b>0.607</b>	<b>0.848</b>	<b>0.007</b>	<b>0.620</b>	<b>0.542</b>	<b>0.774</b>	<b>0.652</b>	<b>0.852</b>	<b>0.018</b>	<b>0.647</b>	<b>0.543</b>

Table 1. Quantitative comparisons on MoCA-Mask and CAD datasets. The top three results are highlighted in red, green, and blue.

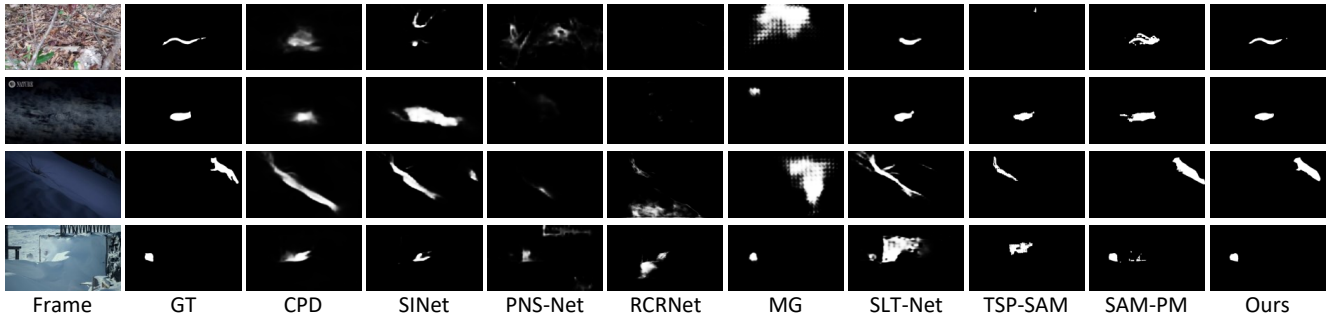


Figure 4. Visualization of our proposed CamoSAM2 and previous state-of-the-art methods on MoCA-Mask and CAD datasets.

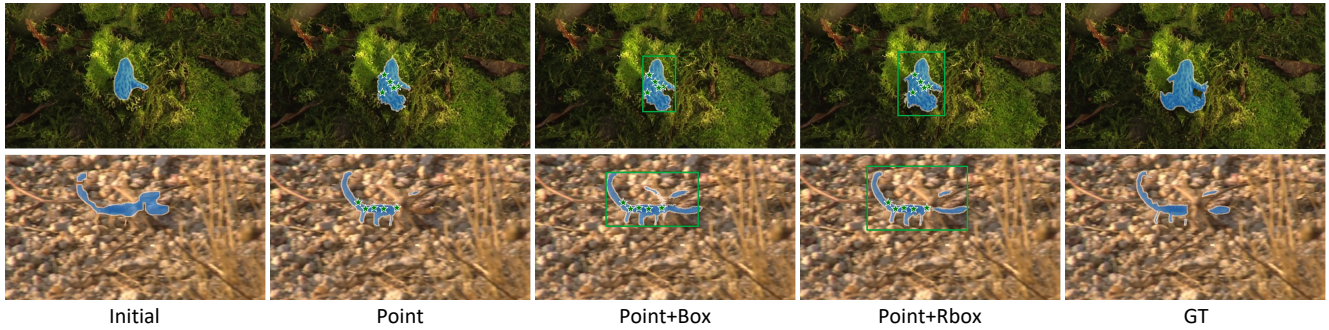


Figure 5. Visualization of our proposed adaptive multi-prompts refinement process. “Initial” represents the coarse masks after preprocessing in Step 1 of Algorithm 1.

Model	Params	FPS	$\mathcal{S}_\alpha \uparrow$	$F_\beta^w \uparrow$	$E_\phi \uparrow$	mDice $\uparrow$
FSPNet [16]	274.24M	2.41	0.565	0.186	0.610	0.238
SLT-Net [5]	<b>82.38M</b>	5.52	0.631	0.311	0.759	0.360
TSP-SAM [18]	727.12M	2.69	0.689	0.044	0.808	0.458
SAM-PM [30]	313.33M	5.08	0.728	0.567	0.813	0.594
CamoSAM2 (ours)	141.56M	<b>6.78</b>	<b>0.765</b>	<b>0.607</b>	<b>0.848</b>	<b>0.620</b>

Table 2. Comparison of model parameters and FPS with state-of-the-art methods. The best scores are highlighted in **bold**.

Model	$\mathcal{S}_\alpha \uparrow$	$F_\beta^w \uparrow$	$E_\phi \uparrow$	$\mathcal{M} \downarrow$	mDice $\uparrow$	mIoU $\uparrow$
Baseline	0.624	0.289	0.781	0.024	0.337	0.251
Appearance	0.631	0.296	0.764	0.024	0.341	0.258
Appearance + Motion	<b>0.670</b>	<b>0.376</b>	<b>0.782</b>	<b>0.014</b>	<b>0.413</b>	<b>0.330</b>

Table 3. Ablation studies of the core components of our proposed MAPI on MoCA-Mask dataset.

Frame	$\mathcal{S}_\alpha \uparrow$	$F_\beta^w \uparrow$	$E_\phi \uparrow$	$\mathcal{M} \downarrow$	mDice $\uparrow$	mIoU $\uparrow$
First	0.627	0.330	0.703	0.046	0.337	0.294
Random	0.629	0.363	0.675	0.065	0.369	0.324
Top-1	<b>0.745</b>	<b>0.561</b>	<b>0.805</b>	<b>0.008</b>	<b>0.570</b>	<b>0.501</b>

Table 4. Comparing different selection methods.

ing the first frame without assessing its relevance is insufficient for guiding accurate segmentation. The ‘‘Random’’ strategy shows moderate results. While its variability occasionally captures useful information, the inconsistency in prompt selection likely limits its effectiveness. The findings underscore the importance of selecting the optimal frame, as it directly impacts the quality and reliability of video segmentation outcomes. See additional illustrations and ablation studies in the [Supp](#) for further evidence supporting the effectiveness of our prompt frame selection strategy.

**Hyper parameter analysis of Top- $k$ .** Table 5 presents the results of using different top  $k$  frames as prompt frames. The settings range from using the top 1 frame (Top-1) to the top 9 frames (Top-9). We observe a performance boost from Top-1 to Top-3, suggesting that incorporating a small number of additional frames enhances SAM2’s ability to generalize the appearance and spatial context of camouflaged objects, thereby improving segmentation quality. Conversely, performance decreases from Top-5 to Top-9, indicating that an excessive number of frames may introduce noise or irrelevant details, particularly when dealing with coarse or inaccurate masks generated by MAPI.

**The number of prompt points.** In Table 6, different numbers of prompt points (denoted as NP) are evaluated, ranging from 1 to 9 points. We can see that the 5 random prompt points (5P) achieve the best performance, representing an optimal balance in prompt input that maximizes segmentation accuracy across all evaluation metrics. Excessive

Setting	$\mathcal{S}_\alpha \uparrow$	$F_\beta^w \uparrow$	$E_\phi \uparrow$	$\mathcal{M} \downarrow$	mDice $\uparrow$	mIoU $\uparrow$
Top-1	0.745	0.561	0.805	0.008	0.570	0.501
Top-3	<b>0.753</b>	<b>0.573</b>	<b>0.822</b>	<b>0.008</b>	<b>0.588</b>	<b>0.515</b>
Top-5	0.743	0.555	0.796	0.008	0.576	0.493
Top-7	0.740	0.551	0.815	0.009	0.567	0.495
Top-9	0.739	0.551	0.811	0.018	0.560	0.490

Table 5. Ablation analysis of the number of Top- $k$  prompt frames on MoCA-Mask dataset.

Model	$\mathcal{S}_\alpha \uparrow$	$F_\beta^w \uparrow$	$E_\phi \uparrow$	$\mathcal{M} \downarrow$	mDice $\uparrow$	mIoU $\uparrow$
1P	0.753	0.573	0.822	0.008	0.588	0.515
3P	0.750	0.572	0.833	0.008	0.588	0.512
5P	0.757	0.582	0.841	0.008	0.597	0.522
7P	0.740	0.551	0.815	0.009	0.567	0.495
9P	0.739	0.548	0.815	0.009	0.566	0.493
box+5P	0.708	0.481	0.771	0.008	0.498	0.430
rbox+5P	<b>0.765</b>	<b>0.607</b>	<b>0.848</b>	<b>0.014</b>	<b>0.620</b>	<b>0.542</b>

Table 6. Ablation studies of different prompt strategies. Here, box denotes using minimum enclosing bounding box; rbox denotes using the refined bounding box proposed by our AMPR.

points (e.g., 7P and 9P) may introduce noise, while too few points (e.g., 1P and 3P) lack sufficient spatial and context information, leading to reduced performance.

**Effectiveness of refined box prompt.** An analysis of the last two rows in Table 6 reveals that the performance of CamoSAM2 does not improve merely by adding diverse prompts. In fact, incorporating box prompts alongside point prompts can degrade segmentation accuracy. This decline is primarily due to the initial box prompts being imperfect, often leading to under-segmentation errors. However, when our refined boxes are introduced, an approximate 3.9% improvement in mDice is observed. This indicates that the quality of the bounding boxes used in conjunction with point prompts plays a critical role in determining segmentation performance, highlighting the model’s sensitivity to the accuracy of box prompt integration. The visualization in Figure 5 further illustrates that our refined bounding boxes capture more detailed information, thereby enriching both global and local contextual understanding of target objects. Overall, these findings underscore the effectiveness of our approach in enhancing segmentation accuracy, especially in scenarios where initial masks are suboptimal.

## 5. Conclusion

In this paper, we introduce CamoSAM2, a novel framework that employs a motion-appearance induced, auto-refining prompt approach to achieve reliable and precise video camouflaged object detection. Our method begins with a motion-appearance prompt inducer module, enabling the detection of camouflaged objects without user-

provided prompts. Moreover, we propose an innovative video-based adaptive multi-prompts refinement strategy, which autonomously produces reliable and robust prompts for high-precision segmentation results, without increasing the number of training parameters. Notably, this strategy is composed of three meticulously designed steps, making it highly suitable for real-world applications. Experimental results on benchmark datasets show that our CamoSAM2 significantly outperforms existing state-of-the-art methods on evaluation metrics and inference speed. Our method offers a new perspective on adapting SAM2 for VCOD task, and we hope it will inspire further research to enhance SAM2’s effectiveness in downstream applications.

## References

- [1] Pia Bideau and Erik Learned-Miller. It’s moving! a probabilistic model for causal motion segmentation in moving camera videos. In *ECCV*, pages 433–449, 2016. 2, 5
- [2] Tianrun Chen, Lanyun Zhu, Chaotao Deng, Runlong Cao, Yan Wang, Shangzhan Zhang, Zejian Li, Lingyun Sun, Ying Zang, and Papa Mao. Sam-adapter: Adapting segment anything in underperformed scenes. In *ICCV*, pages 3367–3375, 2023. 3
- [3] Tianrun Chen, Lanyun Zhu, Chaotao Ding, Runlong Cao, Yan Wang, Zejian Li, Lingyun Sun, Papa Mao, and Ying Zang. Sam fails to segment anything?—sam-adapter: Adapting sam in underperformed scenes: Camouflage, shadow, medical image segmentation, and more. *arXiv preprint arXiv:2304.09148*, 2023. 3
- [4] Tianrun Chen, Ankang Lu, Lanyun Zhu, Chaotao Ding, Chunan Yu, Deyi Ji, Zejian Li, Lingyun Sun, Papa Mao, and Ying Zang. Sam2-adapter: Evaluating & adapting segment anything 2 in downstream tasks: Camouflage, shadow, medical image segmentation, and more. *arXiv preprint arXiv:2408.04579*, 2024. 3, 7
- [5] Xuelian Cheng, Huan Xiong, Deng-Ping Fan, Yiran Zhong, Mehrtash Harandi, Tom Drummond, and Zongyuan Ge. Implicit motion handling for video camouflaged object detection. In *CVPR*, 2022. 1, 2, 3, 4, 5, 6, 7, 8
- [6] Runmin Cong, Mengyao Sun, Sanyi Zhang, Xiaofei Zhou, Wei Zhang, and Yao Zhao. Frequency perception network for camouflaged object detection. In *ACM MM*, pages 1179–1189, 2023. 2
- [7] Deng-Ping Fan, Ming-Ming Cheng, Yun Liu, Tao Li, and Ali Borji. Structure-measure: A New Way to Evaluate Foreground Maps. In *ICCV*, 2017. 6
- [8] Deng-Ping Fan, Cheng Gong, Yang Cao, Bo Ren, Ming-Ming Cheng, and Ali Borji. Enhanced-alignment measure for binary foreground map evaluation. *arXiv preprint arXiv:1805.10421*, 2018. 6
- [9] Deng-Ping Fan, Ge-Peng Ji, Guolei Sun, Ming-Ming Cheng, Jianbing Shen, and Ling Shao. Camouflaged object detection. In *CVPR*, 2020. 7
- [10] Deng-Ping Fan, Ge-Peng Ji, Tao Zhou, Geng Chen, Huazhu Fu, Jianbing Shen, and Ling Shao. Planet: Parallel reverse attention network for polyp segmentation. In *MICCAI*, 2020. 1, 7
- [11] Deng-Ping Fan, Ge-Peng Ji, Ming-Ming Cheng, and Ling Shao. Concealed object detection. *IEEE TPAMI*, 2021. 2, 3, 6, 7
- [12] Deng-Ping Fan, Ge-Peng Ji, Xuebin Qin, and Ming-Ming Cheng. Cognitive vision inspired object segmentation metric and loss function. *SCIENTIA SINICA Informationis*, 2021. 5
- [13] Chunming He, Kai Li, Yachao Zhang, Longxiang Tang, Yulun Zhang, Zhenhua Guo, and Xiu Li. Camouflaged object detection with feature decomposition and edge reconstruction. In *CVPR*, pages 22046–22055, 2023. 2, 7
- [14] Dan Hendrycks and Kevin Gimpel. Gaussian error linear units (gelus). *arXiv preprint arXiv:1606.08415*, 2016. 4
- [15] Yuhao Huang, Xin Yang, Lian Liu, Han Zhou, Ao Chang, Xinrui Zhou, Rusi Chen, Junxuan Yu, Jiongquan Chen, Chaoyu Chen, et al. Segment anything model for medical images? *Medical Image Analysis*, 92:103061, 2024. 3
- [16] Zhou Huang, Hang Dai, Tian-Zhu Xiang, Shuo Wang, Huai-Xin Chen, Jie Qin, and Huan Xiong. Feature shrinkage pyramid for camouflaged object detection with transformers. In *CVPR*, pages 5557–5566, 2023. 3, 7, 8
- [17] Wenjun Hui, Zhenfeng Zhu, Guanghua Gu, Meiqin Liu, and Yao Zhao. Implicit-explicit motion learning for video camouflaged object detection. *IEEE TMM*, pages 1–9, 2024. 2, 5, 7
- [18] Wenjun Hui, Zhenfeng Zhu, Shuai Zheng, and Yao Zhao. Endow sam with keen eyes: Temporal-spatial prompt learning for video camouflaged object detection. In *CVPR*, pages 19058–19067, 2024. 2, 3, 5, 6, 7, 8
- [19] Ge-Peng Ji, Yu-Cheng Chou, Deng-Ping Fan, Geng Chen, Huazhu Fu, Debesh Jha, and Ling Shao. Progressively normalized self-attention network for video polyp segmentation. In *MICCAI*, pages 142–152. Springer, 2021. 7
- [20] Ge-Peng Ji, Guobao Xiao, Yu-Cheng Chou, Deng-Ping Fan, Kai Zhao, Geng Chen, and Luc Van Gool. Video polyp segmentation: A deep learning perspective. *MIR*, 19(6): 531–549, 2022. 1
- [21] Qi Jia, Shuilian Yao, Yu Liu, Xin Fan, Risheng Liu, and Zhongxuan Luo. Segment, magnify and reiterate: Detecting camouflaged objects the hard way. In *CVPR*, pages 4713–4722, 2022. 2
- [22] Abbas Khan, Mustaqeem Khan, Wail Gueaieb, Abdulmoteleb El Saddik, Giulia De Masi, and Fakhri Karray. Camofocus: Enhancing camouflage object detection with split-feature focal modulation and context refinement. In *WACV*, pages 1434–1443, 2024. 2
- [23] Alexander Kirillov, Eric Mintun, Nikhila Ravi, Hanzi Mao, Chloe Rolland, Laura Gustafson, Tete Xiao, Spencer Whitehead, Alexander C Berg, Wan-Yen Lo, et al. Segment anything. In *ICCV*, pages 4015–4026, 2023. 2, 3
- [24] Hala Lamdouar, Charig Yang, Weidi Xie, and Andrew Zisserman. Betrayed by motion: Camouflaged object discovery via motion segmentation. In *ACCV*, 2020. 1, 2
- [25] Shijie Lian and Hua Li. Evaluation of segment anything model 2: The role of sam2 in the underwater environment. *arXiv preprint arXiv:2408.02924*, 2024. 2

- [26] Thomas Lidbetter. Search and rescue in the face of uncertain threats. *European Journal of Operational Research*, 285(3): 1153–1160, 2020. 1
- [27] Ting Liu, Yao Zhao, Yunchao Wei, Yufeng Zhao, and Shikui Wei. Concealed object detection for activate millimeter wave image. *IEEE Transactions on Industrial Electronics*, 66(12): 9909–9917, 2019. 1
- [28] Jun Ma, Yuting He, Feifei Li, Lin Han, Chenyu You, and Bo Wang. Segment anything in medical images. *Nature Communications*, 15(1):654, 2024. 3
- [29] Ran Margolin, Lihi Zelnik-Manor, and Ayellet Tal. How to evaluate foreground maps? In *CVPR*, 2014. 6
- [30] Muhammad Nawfal Meeran, Bhanu Pratyush Mantha, et al. Sam-pm: Enhancing video camouflaged object detection using spatio-temporal attention. In *CVPR*, pages 1857–1866, 2024. 2, 3, 5, 6, 7, 8
- [31] Haiyang Mei, Ge-Peng Ji, Ziqi Wei, Xin Yang, Xiaopeng Wei, and Deng-Ping Fan. Camouflaged object segmentation with distraction mining. In *CVPR*, pages 8772–8781, 2021. 2
- [32] Youwei Pang, Xiaoqi Zhao, Tian-Zhu Xiang, Lihe Zhang, and Huchuan Lu. Zoom in and out: A mixed-scale triplet network for camouflaged object detection. In *CVPR*, pages 2160–2170, 2022. 3, 7
- [33] Adam Paszke, Sam Gross, Francisco Massa, Adam Lerer, James Bradbury, Gregory Chanan, Trevor Killeen, Zeming Lin, Natalia Gimelshein, Luca Antiga, et al. Pytorch: An imperative style, high-performance deep learning library. In *NeurIPS*, 2019. 6
- [34] Federico Perazzi, Philipp Krähenbühl, Yael Pritch, and Alexander Hornung. Saliency filters: Contrast based filtering for salient region detection. In *CVPR*, pages 733–740. IEEE, 2012. 6
- [35] Xuebin Qin, Zichen Zhang, Chenyang Huang, Chao Gao, Masood Dehghan, and Martin Jagersand. Basnet: Boundary-aware salient object detection. In *CVPR*, 2019. 7
- [36] Nikhila Ravi, Valentin Gabeur, Yuan-Ting Hu, Ronghang Hu, Chaitanya Ryali, Tengyu Ma, Haitham Khedr, Roman Rädle, Chloe Rolland, Laura Gustafson, et al. Sam 2: Segment anything in images and videos. *arXiv preprint arXiv:2408.00714*, 2024. 2, 3
- [37] Yujia Sun, Shuo Wang, Chenglizhao Chen, and Tian Zhu Xiang. Boundary-guided camouflaged object detection. In *IJ-CAI*, pages 1335–1341, 2022. 7
- [38] Yanguang Sun, Chunyan Xu, Jian Yang, Hanyu Xuan, and Lei Luo. Frequency-spatial entanglement learning for camouflaged object detection. In *ECCV*, pages 343–360. Springer, 2024. 2, 7
- [39] Lv Tang and Bo Li. Evaluating sam2’s role in camouflaged object detection: From sam to sam2. *arXiv preprint arXiv:2407.21596*, 2024. 2
- [40] Lv Tang, Haoke Xiao, and Bo Li. Can sam segment anything? when sam meets camouflaged object detection. *arXiv preprint arXiv:2304.04709*, 2023. 3
- [41] Wenhai Wang, Enze Xie, Xiang Li, Deng-Ping Fan, Kaitao Song, Ding Liang, Tong Lu, Ping Luo, and Ling Shao. Pvt v2: Improved baselines with pyramid vision transformer. *Computational Visual Media*, 8(3):415–424, 2022. 3, 6
- [42] Junde Wu, Rao Fu, Huihui Fang, Yuanpei Liu, Zhaowei Wang, Yanwu Xu, Yueming Jin, and Tal Arbel. Medical sam adapter: Adapting segment anything model for medical image segmentation. *arXiv preprint arXiv:2304.12620*, 2023. 1
- [43] Yu-Huan Wu, Shang-Hua Gao, Jie Mei, Jun Xu, Deng-Ping Fan, Rong-Guo Zhang, and Ming-Ming Cheng. Jcs: An explainable covid-19 diagnosis system by joint classification and segmentation. *IEEE TIP*, 30:3113–3126, 2021. 1
- [44] Pengxiang Yan, Guanbin Li, Yuan Xie, Zhen Li, Chuan Wang, Tianshui Chen, and Liang Lin. Semi-supervised video salient object detection using pseudo-labels. In *ICCV*, 2019. 7
- [45] Charig Yang, Hala Lamdouar, Erika Lu, Andrew Zisserman, and Weidi Xie. Self-supervised video object segmentation by motion grouping. In *ICCV*, 2021. 1, 7
- [46] Siyuan Yao, Hao Sun, Tian-Zhu Xiang, Xiao Wang, and Xiaochun Cao. Hierarchical graph interaction transformer with dynamic token clustering for camouflaged object detection. *IEEE TIP*, 33:5936–5948, 2024. 2, 7
- [47] Qiang Zhai, Xin Li, Fan Yang, Chenglizhao Chen, Hong Cheng, and Deng-Ping Fan. Mutual graph learning for camouflaged object detection. In *CVPR*, pages 12997–13007, 2021. 2
- [48] Yi Zhang, Jing Zhang, Wassim Hamidouche, and Olivier Deforges. Predictive uncertainty estimation for camouflaged object detection. *IEEE TIP*, 2023. 7
- [49] Jia-Xing Zhao, Jiang-Jiang Liu, Deng-Ping Fan, Yang Cao, Jufeng Yang, and Ming-Ming Cheng. Egnnet: edge guidance network for salient object detection. In *ICCV*, 2019. 7
- [50] Yijie Zhong, Bo Li, Lv Tang, Senyun Kuang, Shuang Wu, and Shouhong Ding. Detecting camouflaged object in frequency domain. In *CVPR*, pages 4504–4513, 2022. 2
- [51] J Zhu, Y Qi, and J Wu. Medical sam 2: Segment medical images as video via segment anything model 2. *arxiv 2024. arXiv preprint arXiv:2408.00874*, 2024. 2, 3